ACS APPLIED MATERIALS & INTERFACES

Research Article

www.acsami.org

Hierarchical Graphene-Encapsulated Hollow SnO_2@SnS_2 Nanostructures with Enhanced Lithium Storage Capability

Wangwang Xu,[†] Zhiqiang Xie,[†] Xiaodan Cui,[†] Kangning Zhao,[‡] Lei Zhang,[‡] Grant Dietrich,[†] Kerry M. Dooley,[§] and Ying Wang*[,†]

[†]Department of Mechanical & Industrial Engineering, Louisiana State University, Baton Rouge, Louisiana 70803, United States

[‡]State Key Laboratory of Advanced Technology for Materials Synthesis and Processing, Wuhan University of Technology, Wuhan 430070, China

[§]Department of Chemical Engineering, Louisiana State University, Baton Rouge, Louisiana 70803, United States

Supporting Information

ABSTRACT: Complex hierarchical structures have received tremendous attention due to their superior properties over their constitute components. In this study, hierarchical graphene-encapsulated hollow SnO_2@SnS_2 nanostructures are successfully prepared by in situ sulfuration on the backbones of hollow SnO_2 spheres via a simple hydrothermal method followed by a solvothermal surface modification. The as-prepared hierarchical SnO_2@SnS_2@rGO nanocomposite can be used as anode material in lithium ion batteries, exhibiting excellent cyclability with a capacity of 583 mAh/g after 100 electrochemical cycles at a specific current of 200 mA/g. This material shows a very low capacity fading of only 0.273% per cycle from the second to the 100th cycle, lower than the capacity degradation of bare SnO_2 hollow spheres (0.830%) and single SnS_2 nanosheets (0.393%). Even after being cycled at a range of specific currents varied from 100 mA/g to 2000 mA/g, hierarchical SnO_2@SnS_2@rGO nanocomposites maintain a reversible capacity of 664 mAh/g, which is much higher than single SnS_2 nanosheets (374 mAh/g) and bare SnO_2 hollow spheres (177 mAh/g). Such significantly improved electrochemical performance can be attributed to the unique hierarchical hollow structure, which not only effectively alleviates the stress resulting from the lithiation/delithiation process and maintaining structural stability during cycling but also reduces aggregation and facilitates ion transport. This work thus demonstrates the great potential of hierarchical SnO_2@SnS_2@rGO nanocomposites for applications as a high-performance anode material in next-generation lithium ion battery technology.

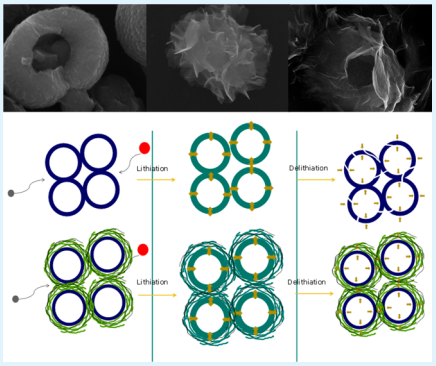

KEYWORDS: *tin dioxide, tin disulfide, hierarchical nanostructure, graphene, anode, lithium ion battery*

1. INTRODUCTION

The ever-increasing consumer market of portable electronic devices has stimulated the need for high-performance energy storage devices.[1−4] Lithium ion batteries (LIBs), as the most widely used energy storage devices, have dominated the market of commercial energy storage for more than two decades due to their high energy density, long cycle life, and environmental friendliness.[5−8] The constructuction of superior LIBs requires that many factors be taken into account, such as high energy density, large capacity with high voltage, and long cycling life.[9−15] Tin and tin-based materials have been extensively studied as anodes since 1997. They are deemed as potential alternatives to replace commercial graphite anodes owing to their advantages of low voltage and high theoretical specific capacity of over 650 mAh/g, which is more than twice that of a commercial graphite anode (372 mAh/g).[16−18] Unfortunately, commercialization of tin and tin-based anodes in current lithium ion batteries is limited by mechanical integrity degradation and short electrochemical cycling life of these materials due to their large volume change up to ∼250% leading to pulverization during Li-ion insertion/extraction processes.[19,20] One approach to solve this issue is to avoid conversion reactiond (Sn to SnO and SnO_2) with a lower voltage limit during electrochemical cycling to maintain cycling stability. Such a method is promising, but the exploited capacity is as low as 365 mAh/g.[21]

Recently, tin or tin compound (SnO, SnO_2, SnS_2, et al.) nanostructures have been explored to alleviate the problems of fragile structure and large volume expansion during lithiation/delithiation.[22,23] For these drawbacks to be overcome, tin-based materials with various morphologies and structures have been obtained over the past few years, including hollow spheres, nanorod arrays, nanobelts, nanosheets, and nanotubes.[24−29] For example, Lou et al. prepared SnO_2 hollow spheres using a hydrothermal method according to the inside-out Ostwald ripening mechanism, which displayed an initial capacity of 1140 mAh/g and a capacity of ∼700 mAh/g in the 30th cycle, demonstrating much better electrochemical performance than

Received: July 27, 2015
Accepted: September 21, 2015
Published: September 21, 2015

DOI: 10.1021/acsami.5b06765
ACS Appl. Mater. Interfaces 2015, 7, 22533−22541

pristine SnO_2 nanoparticles that exhibited an initial capacity of 645 mAh/g and retain almost no capacity after 20 cycles.[27] However, commercialization of tin-based electrodes is still hindered by its severe volume change during cycling and intrinsically poor electronic conductivity. Because of its improved mechanical integrity, larger surface area, better permeabilities, and more surface active sites than common nanostructures,[30−35] hierarchical nanostructures have become very appealing as electrodes in energy devices. Wang et al. synthesized ZnO-SnO_2 hiererchical nanosheets exhibiting higher photocatalytic activities for degrading methyl orange than ZnO rods or SnO_2.[36] Mai et al. prepared hierarchical $MnMoO_4$/$CoMoO_4$ heterostructured nanowires, which delivered a much higher capacity and better rate capability than either constituent component.[37]

Both SnO_2 and SnS_2 are typical tin-based compounds that have been widely studied as anode materials in LIBs. Recently, SnS_2/graphene composite materials have received much attention due to their improved accommodation of hosting spaces and enhanced guest accessibility for the diffusion of both Li ions and sodium ions, resulting in excellent cycling performance and rate capability.[38−40] On the contrary, SnO_2 with a higher theoretical capacity (781 mAh/g) than SnS_2 displays worse cycling stability and rate performance due to its severe pulverization upon cycling.[41] Therefore, it is expected that hierarchical SnO_2@SnS_2@rGO nanocomposites can be a battery electrode material with even better electrochemical performance by combining the advantages of each component.

Herein, to combine the merits of SnO_2 hollow spheres with higher specific capacity, layered SnS_2 with better cycling stability, and reduced graphene oxide (rGO) with excellent electronic conductivity, we design and synthesize hierarchical novel SnO_2@SnS_2@rGO hollow spheres via a facile two-step growth process for application as anodes in new-generation lithium-ion batteries. Briefly, SnO_2 hollow spheres are prepared first via a hydrothermal method. Then, SnS_2 nanosheets directly grow on SnO_2 hollow spheres through facile surface sulfurization to form a hierarchical hollow structure, which ensures mechanical integrity and electrical connection between SnO_2 hollow spheres inside and SnS_2 nanosheets and reduced graphene outside. In this structure, both SnS_2 nanosheets and reduced graphene outside serve as the protecting shells for SnO_2 hollows spheres inside from dramatic volume variation during electrochemical cycling, thus alleviating their disintegration and pulverization during lithiation/delithiation. Additionally, the inner hollow space of this structure releases stress resulting from the volume change. Compared to the fragile mechanical property of SnO_2 hollow spheres during lithiation and delithiation, hierarchical SnO_2@SnS_2 hollow spheres can effectively maintain the integrity during cycling (Figure 1). Through being encompassed by SnS_2 nanosheets, hierarchical SnO_2@SnS_2@rGO hollow spheres combine the merits of large discharge capacity and excellent cycling stability from each component to achieve improved cycling stability with a high discharge capacity. In addition, the hierarchical core−shell structure provides good protection of SnO_2 hollow spheres, ensuring excellent structural stability. To improve electronic conductivity and rate capability, and further protect the shell of SnS_2 nanosheets from cracking, we further coated SnO_2@SnS_2 with rGO. The resulting hierarchical SnO_2@SnS_2@rGO hollow spheres are expected to deliver remarkable electrochemical performance. To the best of our knowledge, such novel hierarchical electrode material is obtained for the first time.

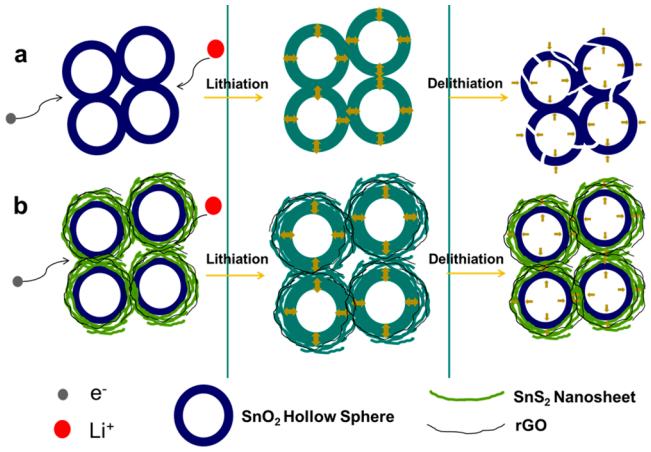

Figure 1. Schematic illustrations of SnO_2 hollow spheres and hierarchical SnO_2@SnS_2@rGO hollow spheres during electrochemical cycling. (a) Structural degradation of SnO_2 hollow spheres during cycling. SnO_2 hollow spheres tend to pulverize. Most SnO_2 hollow spheres crack and crush during cycling, resulting in poor cycling performance. (b) Hierarchical SnO_2@SnS_2@rGO hollow spheres have better permeability and more surface active sites. In this structure, SnS_2 nanosheets and the shells of rGO sheets outside SnO_2 hollow spheres can improve electronic conductivity and provide facile strain relaxation during cycling, allowing them to increase in thickness without pulverization and maintain mechanical integrity.

Owing to the synergic effects of each constituent in the hybrid structure, hierarchical graphene-encapsulated hollow SnO_2@SnS_2 nanostructures demonstrate significant potential for application as anode material in superior lithium-ion batteries.

2. EXPERIMENTAL SECTION

Materials Synthesis. All chemical reagents employed in this study were of analytical grade and used without further purification.

Synthesis of SnO_2 Hollow Spheres. $SnCl_4·5H_2O$ (1.73 g) and NaOH (1.25 g) were dissolved in 30 mL of distilled water under vigorous magnetic stirring for 30 min. The obtained solution was transferred into a Teflon-lined stainless autoclave (50 mL) and heated at 200 °C for 24 h. After cooling to room temperature naturally, the resultant white powder was rinsed with deionized water and ethyl acohol repeatedly, separated by centrifugation, and dried at 60 °C for 8 h.

Synthesis of SnS_2 Nanosheets. $SnCl_4·5H_2O$ (0.54 g) and thiourea (0.49 g) were dissolved in 30 mL of isopropyl alcohol under vigorous magnetic stirring for 30 min. The obtained solution was transferred into a stainless Teflon-lined autoclave and heated at 180 °C for 24 h. After cooling to room temperature naturally, the resultant golden precipitate was collected by centrifugation and rinsed alternatively with deionized water and ethyl alcohol several times.

Synthesis of Hierarchical SnO_2@SnS_2. The as-prepared SnO_2 (0.28 g) and 1.8 g of urea were dispersed in 30 mL of isopropyl alcohol by sonication for 5 min. After magnetic stirring for 30 min, the solution was transferred into a stainless Teflon-lined autoclave (50 mL) and heated at 180 °C for 36 h. After cooling to room temperature naturally, the product was collected via centrifuge and rinsed repeatly.

Synthesis of Hierarchical SnO_2@SnS_2@rGO Hollow Spheres. The as-prepared SnO_2 (0.28 g) was dispersed in 30 mL of isopropyl alcohol by sonication for 5 min. Then, 1.8 g of urea and 5 mL (6 mol/L) of a GO (ACS Material, LLC) dispersion colloid were added to the solution. After magnetic stirring for 30 min, the solution was transferred into a stainless Teflon-lined autoclave (50 mL) and heated at 180 °C for 36 h. The obtained light black product was then reduced in 100 mL of hydrazine hydrate solution with a concentration of 10 mmol/L for ∼3 h. Then, the product was collected by centrifugation and rinsed alternatively with deionized water and ethyl alcohol several

DOI: 10.1021/acsami.5b06765
ACS Appl. Mater. Interfaces 2015, 7, 22533−22541

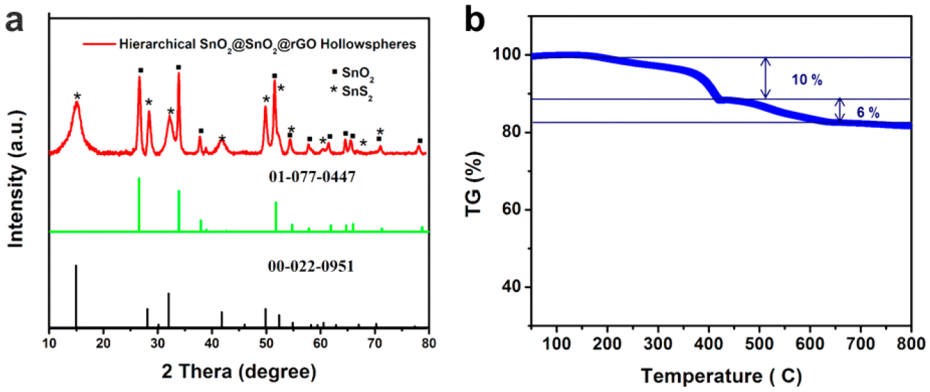

Figure 2. (a) XRD patterns of SnO_2@SnS_2@rGO. (b) TG analysis of SnO_2@SnS_2@rGO in air.

times. The hierarchical SnO_2@SnS_2 hollow spheres were prepared by the same method without adding GO.

Characterization. Crystallographic structures of the obtained products were determined by Rigaku MiniFlex X-ray diffraction (XRD) measurements with Cu Kα radiation in a 2θ range from 10° to 80° at room temperature. Surface morphology, particle size, and energy dispersive spectroscopy (EDS) were studied using an FEI Quanta 3D FEG field emission scanning electron microscope (FESEM). Thermogravimetric (TG) analysis was performed on an SII STA7300 analyzer at a heating rate of 1 °C min^{-1} in air.

Electrochemical Measurements. The anodes were composed of the as-prepared tin-based material (hierarchical SnO_2@SnS_2@rGO hollow spheres, hierarchical SnO_2@SnS_2 hollow spheres, SnO_2 hollow spheres, or SnS_2 nanosheet powders) and acetylene black as well as sodium alginate binder mixed at a weight ratio of 7:2:1 in deionized water followed by drying. The anodes were assembled into CR2032-type coin cells in an argon-filled glovebox using lithium foil as the cathode and celgard-2320 membrane as separator; the electrolyte was 1 M $LiPF_6$ dissolved in ethylene carbonate (EC) and dimethyl carbonate (DMC) and diethylcarbonate (DEC) at a volumetric ratio of 1:1:1. The coin cells were aged for 12 h before electrochemical measurements to ensure full filtration of the electrolyte into the electrodes. Galvanostatic charge/discharge measurements were performed using an eight-channel battery analyzer (MTI Corporation) at a voltage range of 0.01−2 V (versus Li^+/Li). Cyclic voltammetry (CV) measurements were performed using an electrochemical workstation (CHI 6504C) over the potential range of 0.01−2.0 V relative to Li^+/Li at a scanning rate of 0.1 mV/s. Electrochemical impedance spectroscopy (EIS) measurements were conducted by applying an AC potential of 5 mV amplitude in the frequency range from 0.01 to 100 kHz. Thermogravimetric (TG) analysis was performed on an SII STA7300 analyzer at a heating rate of 1 °C/min in nitrogen.

3. RESULTS AND DISCUSSION

For the preparation of hierarchical SnO_2@SnS_2@rGO hollow spheres, SnO_2 hollow spheres are first obtained as described in the Experimental Section. The formation mechanism of the SnO_2 hollow spheres can be attributed to the inside-out Ostwald ripening process.[23]

$$Sn^{4+} + 6OH^- = Sn(OH)_6^{2-} \quad (1)$$

$$Sn(OH)_6^{2-} = SnO_2 + 2H_2O + 2OH^- \quad (2)$$

As shown in reactions 1 and 2, Sn^{4+} will hydrolyze to produce primary SnO_2 nanocrystals. This process is completed very quickly; therefore, these renascent solid spheres might not be crystallized well, especially for the nanoparticles inside. Subsequently, these inner nanoparticles with higher surface energy will dissolve and further hydrolyze and condense to form SnO_2 nanocrystals on the surface of the spheres. A formation mechanism of the hierarchical core−shell structure has been proposed. At the initial stage of suffixation reaction in thiourea solution, H_2S that is released from the decomposition of thiourea adsorbs on the metal surrounding SnO_2 hollow spheres. Then, S atoms interact with the tin atoms and form the surface tin disulfide via O↔S exchange by releasing oxygen atoms at the same time. Finally, sulfur diffuses into lattice along oxygen vacancies and replaces oxide. Because of the relatively lower diffusion coefficient, the diffusion depth of S atoms reaches its limit at a certain thickness. Moreover, the sulfuration product SnS_2 tends to nucleate and grow on the reaction sites on the surface of SnO_2 because the energy of nucleation required in the heterogeneous phase is generally lower than that in the homogeneous phase. With the sulfuration process progressing, SnS_2 nanosheets are produced that encapsulate the rest of the SnO_2 hollow spheres. SnO_2 hollow spheres are not only used as a source of tin but also as the "substrate" guiding the self-assembly growth of SnS_2 in aqueous solution without surfactant or stabilizers. Moreover, as they have a typical layered structure, SnS_2 nanosheets are easily self-assembled around SnO_2 hollow spheres to form hierarchical SnO_2@SnS_2 hollow spheres. The reason that SnO_2@SnS_2 can be wrapped with graphene is clarified below. During the hydrothermal process, the outer electron orbit of the Sn element can bond with the π electron cloud and the residual oxygen-containing functional groups of graphene. In addition, SnS_2 is structurally and morphologically analogous to graphene. Therefore, rGO tends to wrap around the surface of SnO_2@SnS_2 during the hydrothermal process to significantly reduce the high surface energy.

Figure 1 compares the schematic view of a possible structural change of SnO_2 hollow spheres and hierarchical SnO_2@SnS_2@rGO nanostructures during repeated lithiation/delithiation processes. It can be seen that SnO_2 hollow spheres tend to crack, crush, and pulverize during electrochemical cycling, resulting in structural degradation and poor cycling performance (Figure 1a). However, the hierarchical SnO_2@SnS_2@rGO structure is very promising for delivering excellent electrochemical performance due to the following reasons: First, compared to the easy breaking up of bare SnO_2 hollow spheres during cycling due to their large volume variations in Figure 1a, hierarchical SnO_2@SnS_2@rGO hollow spheres, with SnO_2 hollow spheres encapsulated by SnS_2@rGO nanosheets on the outside, can effectively relieve the pressure resulting from outward expansion during intercalation of lithium ions into the interior of anode materials, leading to improved mechanical

DOI: 10.1021/acsami.5b06765
ACS Appl. Mater. Interfaces 2015, 7, 22533−22541

integrity (Figure 1b). Second, the designed hierarchical structure with enhanced permeability and larger specific surface areas provides more pathways for lithium ion transport, resulting in more facile and faster lithium ion transport. Meanwhile, with the rGO sheets surrounding the spheres, faster reaction kinetics of hierarchical SnO_2@SnS_2@rGO hollow spheres is realized.

To determine crystal structures of hierarchical SnO_2@SnS_2@rGO hollow spheres, hierarchical SnO_2@SnS_2 hollow spheres, SnO_2 hollow spheres, and SnS_2 nanosheets, we conducted X-ray diffraction (XRD) measurements. Figure 2 and Figure S1 (Supporting Information (SI)) present the XRD patterns of hierarchical SnO_2@SnS_2@rGO hollow spheres and each single component, respectively. Regarding the backbones of SnO_2 hollow spheres, their XRD pattern in Figure S1a is identified as tetragonal SnO_2 with lattice parameters of a = 4.7358 Å, b = 4.7358 Å, c = 3.1851 Å, $P42/mnm$ space group, which matches well with the standard XRD pattern of tetragonal cassiterite SnO_2 (JCPDF card no. 01-077-0447). As for pristine SnS_2 nanosheets, its XRD pattern (Figure S1b) is identified as hexagonal berndtite SnS_2 (JCPDF card no. 00-022-0951) with lattice parameters of a = 3.6486 Å, b = 3.6486 Å, c = 5.8992 Å, $P\bar{3}m1$ space group. The XRD patterns of both hierarchical SnO_2@SnS_2 (Figure S1c) and hierarchical SnO_2@SnS_2@rGO (Figure 2a) display the crystallinity combination of bare SnO_2 hollow spheres and layered SnS_2 nanosheets, suggesting the formation of SnO_2@SnS_2 heterostructure. It is noted that there are no obvious diffraction peaks from rGO due to its low crystallinity. Then, thermogravimetric (TG) measurements are performed to further investigate the content of each component in the hierarchical material. The TG curve of SnO_2@SnS_2@rGO composite in Figure 2b shows two main steps corresponding to oxidizations of SnS_2 nanosheets and rGO, respectively. Combustion of SnS_2 nanosheets starts at ~250 °C and completes at ~425 °C. The calculated weight loss is 10%, which is ascribed to 56 wt % SnS_2 in the sample. Combustion of rGO starts at ~500 °C and completes at 650 °C, corresponding to a 6% weight loss in the second step and 6 wt % rGo in the sample.

Figure 3 and Figure S2 present SEM images of the as-prepared SnO_2 hollow spheres, hierarchical SnO_2@SnS_2 hollow spheres, hierarchical SnO_2@SnS_2@rGO hollow spheres, and SnS_2 nanosheets. Figure 3a shows a typical SEM image of the as-synthesized SnO_2 nanospheres at low magnification. Large quantities of smooth-faced SnO_2 nanospheres with diameters of ~1 μm can be clearly observed. Additionally, the high-magnification SEM image in Figure 3b displays a broken SnO_2 sphere, proving that the as-prepared SnO_2 spheres are hollow. The hollow sphere is also shown to have an inner diameter of 400 nm with a thickness of ~300 nm. For hierarchical SnO_2@SnS_2 hollow spheres to be obtained, the as-prepared SnO_2 reacts with thiourea for 36 h. Figure 3c displays an SEM image of hierarchical SnO_2@SnS_2 hollow spheres at low magnification. It can be seen that each sphere is separated by nanosheets, indicating that aggregation of SnO_2 hollow spheres is effectively prevented by the sulfuration process. In the high-magnification SEM image, it is shown that SnO_2 hollow spheres are completely encapsulated by SnS_2 nanosheets, which directly grow on the surface of SnO_2 hollow spheres via in situ surface sulfurization. To further study the elemental composition and distribution, we performed EDS mapping. It is clearly observed in Figure S3 that hierarchical SnO_2@SnS_2 hollow spheres consist of Sn, S, and O. The EDS

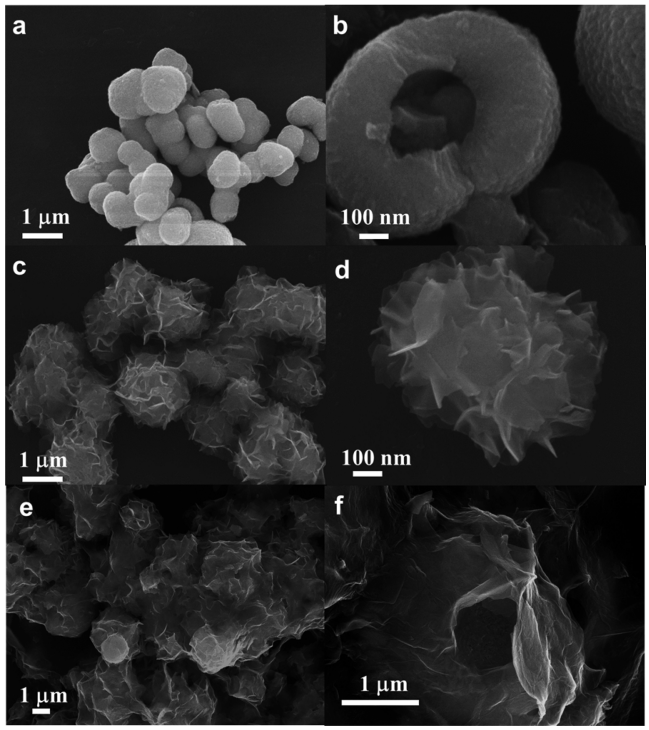

Figure 3. (a) SEM image and (b) magnified SEM image of SnO_2; (c) SEM image and (d) magnified SEM image of SnO_2@SnS_2; and (e) SEM image and (f) magnified SEM image of SnO_2@SnS_2@rGO.

line scan (inset in Figure S3) confirms that the oxygen element is distributed much narrower than sulfur, indicating that the oxygen element is inside and SnO_2 hollow spheres are completely encapsulated by SnS_2 nanosheets. For comparison purposes, SnS_2 nanosheets are prepared and investigated as a reference sample to compare with the performance of the composite material. Figure S2 displays SEM images of single SnS_2 nanosheets. Figure S2a shows that the as-prepared SnS_2 nanosheets are quite homogeneous, forming flowerlike shapes. The magnified image (Figure S2b) reveals that SnS_2 nanosheets are approximately a few nanometers thick and ~2 μm long. For hierarchical SnO_2@SnS_2@rGO hollow spheres to be formed, rGO nanosheets are yielded via reduction of GO nanosheets. As shown in the SEM image at low magnification, most of the hierarchical SnO_2@SnS_2 hollow spheres are encompassed by rGO, together forming integrated electron transport, which can effectively improve the rate capability of the sample. It can be seen from the magnified SEM image (Figure 3f) that each sphere is surrounded completely by rGO in the hierarchical SnO_2@SnS_2@rGO hollow structure. SnS_2 and rGO serve as the shell layer outside SnO_2 hollow spheres for protection. Moreover, the composition of the hierarchical SnO_2@SnS_2@rGO hollow structure is also determined by EDS. As seen in the EDS mapping in Figure S4, hierarchical SnO_2@SnS_2@rGO hollow spheres are composed of C, O, S, and Sn, which confirms successful fabrication of this novel battery electrode material.

To further identity the hierarchical structure of the as-prepared samples, we carried out TEM and HR-TEM coupled with electron diffraction characterizations. As shown in Figure 4a, the SnO_2@SnS_2 core−shell structure is identified, wherein the inner hollow sphere is completely encapsulated by the surrounding nanosheets. The HR-TEM image of nanosheets in Figure 4b exhibits lattice fringes with spacings of 5.89, 2.95, and

DOI: 10.1021/acsami.5b06765
ACS Appl. Mater. Interfaces 2015, 7, 22533−22541

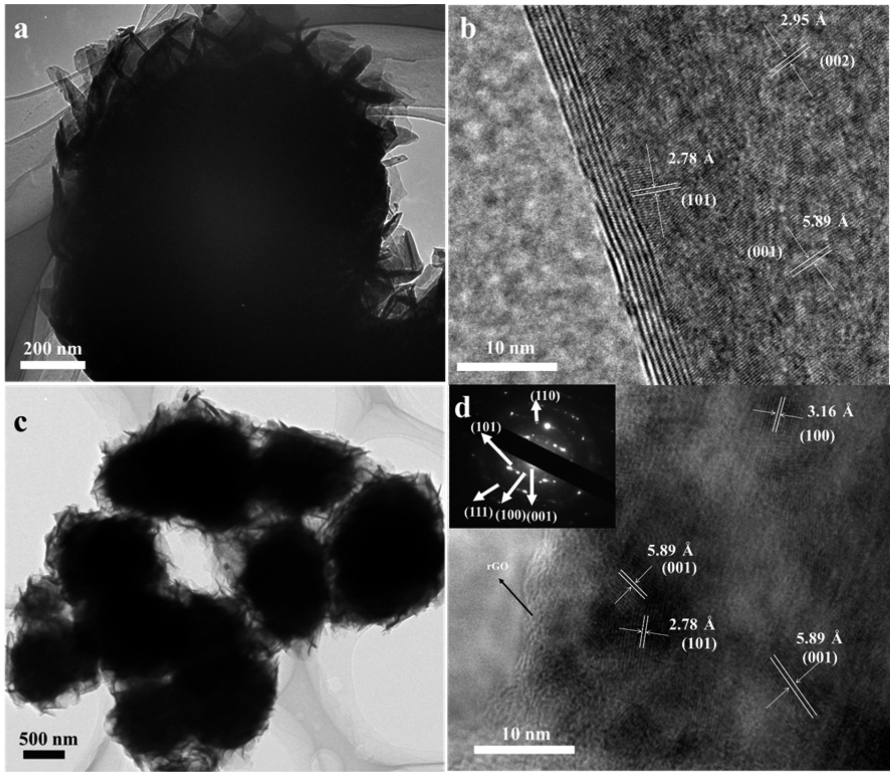

Figure 4. TEM image (a) and HRTEM image (b) of hierarchical SnO_2@SnS_2 hollow spheres; TEM image (c) and HRTEM image (d) of hierarchical SnO_2@SnS_2@rGO hollow spheres with corresponding SAED.

2.78 Å, which can be assigned to the (001), (002), and (101) planes of SnS_2, respectively. In addition, the TEM image in Figure 4c further confirms the hierarchical structure of the SnO_2@SnS_2@rGO sample. The lattice fringes with spacings of 5.89, 3.16, and 2.78 Å are determined in the HRTEM image in Figure 4d, corresponding to the (001), (100), and (101) planes of SnS_2, respectively. Moreover, it can be clearly observed that SnS_2 nanosheets are completely coated with an amorphous film, which is recognized as rGO. A selected-area electron diffraction (SAED) pattern in Figure 4d is well-indexed as a hexagonal SnS_2 phase. In addition, to evaluate the specific surface area, the N_2 adsorption−desorption measurements of all the samples are perfomed. Hierarchical SnO_2@SnS_2@rGO hollow spheres display a Brunauer−Emmett−Teller (BET) surface area of 29.32 m^2/g, which is larger than that of SnO_2@SnS_2 hollow spheres (25.0 m^2/g) and bare SnO2 hollow spheres (11.9 m^2/g).

For the electrochemical performances of all the samples to be evaluated, coin cells of hierarchical SnO_2@SnS_2@rGO hollow spheres, hierarchical SnO_2@SnS_2 hollow spheres, SnO_2 hollow spheres, and SnS_2 nanosheets were assembled and cycled in a voltage range of 0.01−2 V (versus Li^+/Li). Generally, electrochemical reactions of SnO_2 and SnS_2 with lithium can be described as

$$SnO_2 + 4Li = 2Li_2O + Sn \quad (3)$$

$$SnS_2 + 4Li = 2Li_2S + Sn \quad (4)$$

$$Sn + xLi^+ + xe^- = Li_xSn \quad (5)$$

Reactions 3 and 4 are regarded as partially reversible. Therefore, theoretical capacities of SnO_2 and SnS_2 are determined to be 782 and 650 mAh/g, respectively, based on reaction 5. Figure S5a displays CV curves of SnO_2 hollow spheres showing two characteristic peaks at 0.9 and 0.1 V relative to Li/Li^+ in the first potential sweeping cycle, which are ascribed to decomposition of SnO_2 into metallic Sn and Li_2S (reaction 3) and generation of Li−Sn alloy (reaction 5), respectively. It is noted that the decomposition reaction is partially reversible. In subsequent cycles, intercalation of lithium ions occurs at 0.1 V and deintercalation of lithium ions occurs at 0.5 V relative to Li/Li^+ due to the alloying/dealloying reactions (reaction 5). An additional cathodic peak at 0.9 V and anodic peak at 1.3 V can be attributed to the partially reversible conversion process (reaction 3). The CV curves of SnS_2 nanosheets in Figure S5c exhibit three characteristic peaks at 1.7, 1.2, and 0.1 V in the first potential sweeping cycle, which are attributed to lithium intercalation of SnS_2 layers without phase decomposition, decomposition of SnS_2 into metallic Sn and Li_2S (reaction 4), and generation of a Li−Sn alloy, respectively. In subsequent cycles, the redox peaks at 0.1 V in the anodic reaction and 0.6 V in the cathodic reaction can be ascribed to the reversible alloying and dealloying reactions of Sn and Li (reaction 5), respectively. In the CV curves of hierarchical SnO_2@SnS_2@rGO hollow spheres (Figure 5a), four broad peaks appear at the potentials 1.7, 1.2, 0.9, and 0.1 V in the first potential sweeping cycle. The peak at ~1.7 V can be attributed to lithium intercalation of SnS_2 layers without phase decomposition. The peaks around 1.2 and 0.9 V are attributed to the conversion reactions of SnO_2 (reaction 3) and SnS_2 (reaction 4), respectively. The peak at 0.1 V is related to the generation of the Li−Sn alloy. It can be seen that both CV curves display characteristic peaks of SnO_2 hollow spheres and SnS_2 nanosheets, confirming the coexistence of SnO_2 and SnS_2 in the samples.

DOI: 10.1021/acsami.5b06765
ACS Appl. Mater. Interfaces 2015, 7, 22533−22541

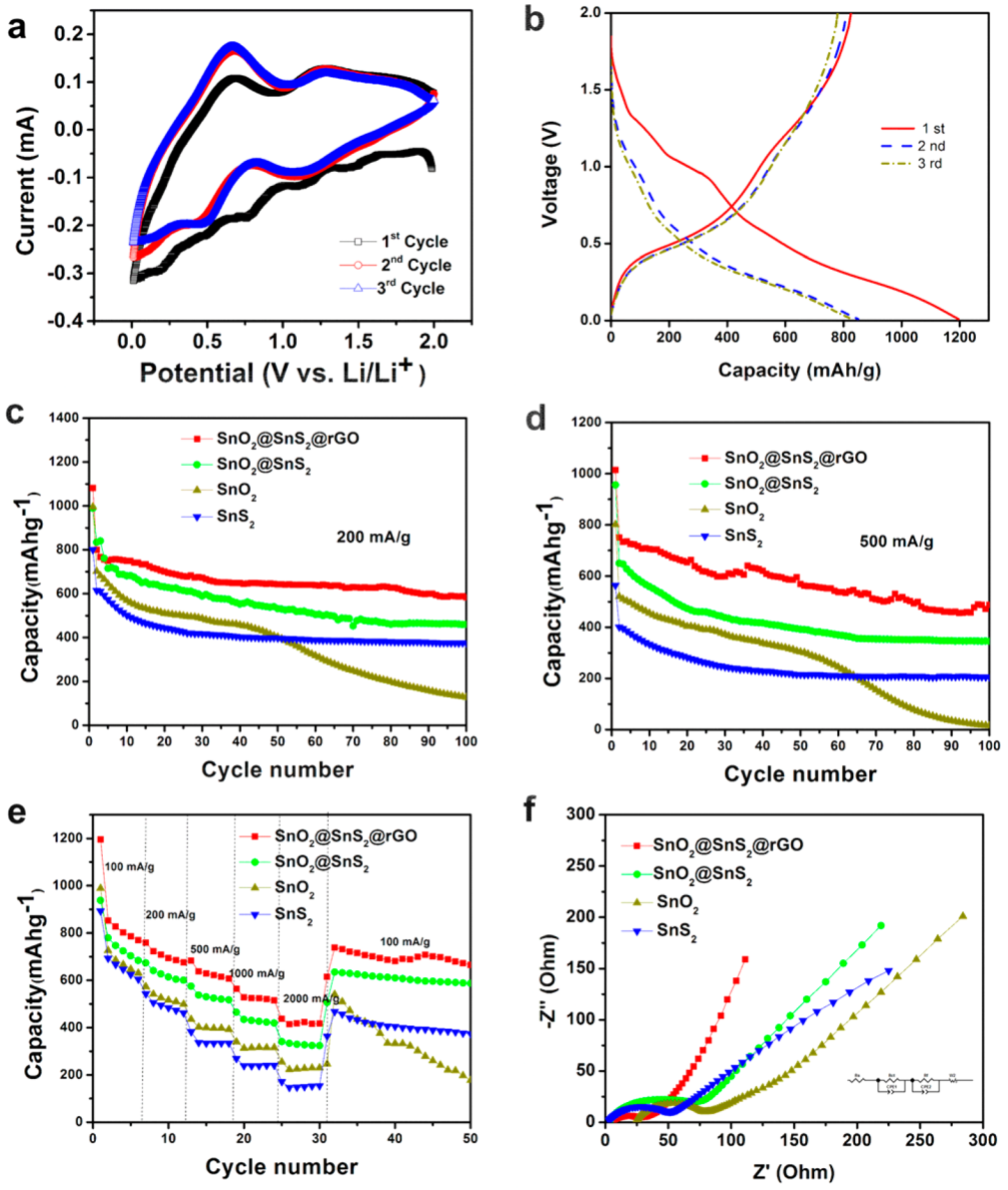

Figure 5. (a) CV curves and (b) galvanostatic charge−discharge profiles of the first three cycles of hierarchical SnO_2@SnS_2 hollow spheres. (c, d) Cycling performance of hierarchical SnO_2@SnS_2@rGO hollow spheres, hierarchical SnO_2@SnS_2 hollow spheres, SnO_2 hollow spheres, and SnS_2 nanosheets at specific currents of 200 and 500 mAh/g, respectively. (e) Rate performances of hierarchical SnO_2@SnS_2@rGO hollow spheres, hierarchical SnO_2@SnS_2 hollow spheres, SnO_2 hollow spheres, and SnS_2 nanosheets at specific currents of 100, 200, 500, 1000, 2000 mA/g and back to 100 mA/g. (f) Nyquist plots of hierarchical SnO_2@SnS_2@rGO hollow spheres, hierarchical SnO_2@SnS_2 hollow spheres, SnO_2 hollow spheres, and SnS_2 nanosheets at 100% depth.

The charge and discharge characteristics of hierarchical SnO_2@SnS_2@rGO hollow spheres are investigated between 0.01 and 2.0 V relative to Li/Li^+ at a specific current of 100 mA/g (Figure 5b). The first discharge and charge capacities of hierarchical SnO_2@SnS_2@rGO hollow spheres are approximately 1195 and 826 mAh/g. The potential plateaus at 1.25 and 1.0 V are ascribed to the conversion reaction between SnO_2, SnS_2, and Li^+, leading to the formation of Li_2O, Li_2S, and Sn in the first discharge process. The following profiles with long slope indicate generation of the Li−Sn alloy (reaction 5).

Panels c and d in Figure 5 summarize the cycling performances of hierarchical SnO_2@SnS_2@rGO hollow spheres, hierarchical SnO_2@SnS_2 hollow spheres, SnO_2 hollow spheres, and SnS_2 nanosheets. When the specific current is 200 mA/g (Figure 5c), the initial discharge capacity of hierarchical SnO_2@SnS_2@rGO hollow spheres is as high as 1150 mAh/g. However, very rapid capacity decay is observed for all four samples, which is generally mainly due to partial reversibility of reactions 3 and 4 and generation of a solid electrolyte interface (SEI) associated with decomposition of the electrolyte.[33,34] After 100 electrochemical cycles, the hierarchical SnO_2@SnS_2@rGO sample maintains a capacity of 583 mAh/g, corresponding to a capacity fading of 0.273% per cycle from the second to the 100th cycle, demonstrating an outstanding cycling stability. In contrast, a drastic capacity fading is observed for pristine SnO_2 hollow spheres after 50 cycles, corresponding to a capacity fading of as high as 0.830% per cycle from the second to 100th cycle. This result may be caused by expansion/contraction of SnO_2 hollow spheres during charge/discharge, leading to severe pulverization and delamination of the conductive substrate.

DOI: 10.1021/acsami.5b06765
ACS Appl. Mater. Interfaces 2015, 7, 22533−22541

Meanwhile, SnS_2 nanosheets exhibit a lower initial discharge capacity at ~800 mAh/g and stable cycling performance with a capacity fading as high as 0.393% per cycle from the second to the 100th cycle. These may be attributed to the low theoretical capacity of SnS_2 nanosheets and stable layered structure of SnS_2 with hosting space for swelling accommodation. In comparison with pristine SnO_2 and SnS_2 nanosheets, both hierarchical SnO_2@SnS_2 hollow spheres and hierarchical SnO_2@SnS_2@rGO hollow sphere anodes display a larger discharge capacity and longer cycling life, which is attributed to unique hierarchical structure with higher permeability, reduced aggregation, and better mechanical integrity. Compared to the specific discharge capacity of 450 mAh/g of the hierarchical SnO_2@SnS_2 hollow structure after 100 electrochemical cycles, hierarchical SnO_2@SnS_2@rGO hollow spheres display a capacity of 583 mAh/g, showing a higher discharge capacity and capacity retention attributed to the rGO layer wrapped outside, which not only protects the inner active material from volume change during cycling but also promotes facile electron transport and prohibits the formation of an SEI film.

When the specific current is increased to 500 mA/g, enhanced cycling performance is also obtained. Compared with hierarchical SnO_2@SnS_2 hollow spheres (345 mAh/g), SnO_2 hollow spheres (15 mAh/g), and SnS_2 nanosheets (206 mAh/g) (Figure 5d), hierarchical SnO_2@SnS_2@rGO hollow spheres deliver a discharge capacity of 487 mAh/g after 100 cycles, showing the highest discharge capacity and best cycling performance. The rate performances of the as-prepared samples are summarized in Figure 5e. Hierarchical SnO_2@SnS_2@rGO hollow spheres deliver a discharge capacity of 1195, 722, 637, 527, and 436 mAh/g at specific currents of 100, 200, 500, 1000, and 2000 mA/g, respectively, as shown in Figure 5e. When the specific current goes back to 100 mA/g, the discharge capacity is recovered to 664 mAh/g, showing the best rate capability among hierarchical SnO_2@SnS_2 (587 mAh/g), pure SnO_2 hollow spheres (177 mAh/g), and pure SnS_2 nanosheets (370 mAh/g). Hierarchical SnO_2@SnS_2@rGO hollow spheres exhibit improved rate capability due to good mechanical integrity of hierarchical structure during fast lithium intercalation and deintercalation. Moreover, rGO sheets wrapping around SnS_2 nanosheets provide a continuous pathway for fast electron transport, as confirmed by the EIS results in Figure 5f. EIS technology, one of the most powerful tools for studying electrochemical kinetics, can be used to investigate the processes occurring at the electrode/electrolyte interfaces and Li^+ intercalation/deintercalation within electrode materials in the battery cells. In the Nyquist plots, R_Ω represents the Ohmic resistance of the battery cell, including electrodes, electrolytes, and other cell components. R_{ct} represents the charge transfer resistance. CPE and Z_w are the double layer capacitance and the Warburg impedance, respectively (Figure 4f). All the Nyquist plots are composed of a depressed semicircle in the medium-frequency region followed by a slanted line in the low-frequency region. The electrode of hierarchical SnO_2@SnS_2@rGO hollow spheres shows the lowest charge transfer resistance of 30 Ω compared to those of hierarchical SnO_2@SnS_2@rGO hollow spheres (75 Ω), SnO_2 hollow spheres (80 Ω), and SnS_2 nanosheets (50 Ω), indicating a faster charge transfer at the electrode/electrolyte interface. Specifically, as observed in Figure 4, the SnO_2 sample shows higher capacity but worse cycling stability than bare SnS_2. On the contrary, the SnS_2 sample exhibits relatively low capacity but much better cycling stability than SnO_2. Therefore, the SnO_2@SnS_2 composite combines the merits of both SnO_2 and SnS_2, resulting in higher capacity and better cycling stability than either individual component. In addition, graphene has been widely reported to effectively improve electrical conductivity of the overall electrode and can also serve as promising protection for the SnO_2@SnS_2 active material to restrict large volume change upon cycling. Therefore, in this work, the graphene-encapsulated hollow SnO_2@SnS_2 sample exhibits the highest specific capacity and the best cycling stability and rate capability among the four anodes (SnO_2, SnS_2, SnO_2@SnS_2, and SnO_2@SnS_2@graphene). Such significantly improved electrochemical performance can be ascribed to the synergic effect of each component in the composite. In addition, compared with most recently reported SnO_2- or SnS_2-based nanostructure anode materials (as shown in Table S1), our work demonstrates significantly improved discharge capacity and prolonged cycling life even at higher specific currents. For example, Guo et al.[42] reported that the SnO_2@graphene composite can retain only 433 mAh/g after 20 cycles at a specific current of 100 mA/g. The SnS_2 nanosheets@multiwalled carbon nanotubes composite material can maintain only 400 mAh/g after 50 cycles at a specific current of 100 mA/g.[45]

In this work, the enhanced electrochemical performance of hierarchical SnO_2@SnS_2@rGO hollow spheres is mainly due to the following reasons: (1) The merits of SnO_2 hollow spheres with higher specific capacity and layered SnS_2 with better cycling stability are revealed in the hierarchical SnO_2@SnS_2@rGO hollow structure. (2) In the hierarchical core−shell hollow structure, SnS_2@rGO shells stabilize the inner SnO_2 hollow spheres, which effectively alleviate the stress by local empty space to achieve excellent structural stability and mechanical integrity. (3) The hierarchical structure provides reduced aggregation, large surface area, better permeability, and more available charge storage sites, contributing to superior kinetics and excellent rate capability as well as enhanced cycling performance. Table S1 compares the cycling performance of our hierarchical hollow SnO_2@SnS_2@rGO nanostructure with various SnO_2- or SnS_2-based nanostructure electrodes reported in the literature,[42−47] and it is found that hierarchical SnO_2@SnS_2@rGO hollow spheres display obviously prolonged cycling life and increased specific discharge capacity as well as improved rate capability when cycled at a specific current of 200 mA/g. Therefore, such novel hierarchical SnO_2@SnS_2@rGO hollow spheres are very promising for application as a superior electrode material in new-generation lithium-ion batteries due to their easy preparation and excellent electrochemical performance.

4. CONCLUSIONS

In summary, hierarchical SnO_2@SnS_2@rGO hollow spheres are successfully synthesized by a facile and scalable in situ sulfuration method that involves a simple hydrothermal treatment followed by a solvothermal process. When assembled into lithium-ion battery cells, the as-prepared material delivers a specific capacity of 583 mAh/g after 100 cycles at a specific current of 200 mA/g and a reversible capacity of 664 mAh/g after being cycled at a high specific current of 2000 mA/g, demonstrating a significantly increased capacity and enhanced cycling reversibility compared to either bare SnO_2 hollow spheres or SnS_2 nanosheets. Because of their unique hierarchical hollow structure, the as-prepared hierarchical SnO_2@SnS_2@rGO hollow spheres can effectively alleviate stress and accommodate a large volume change during the

DOI: 10.1021/acsami.5b06765
ACS Appl. Mater. Interfaces 2015, 7, 22533−22541

lithiation/delithiation process, leading to excellent structural stability and mechanical integrity. This structure also provides continuous pathways for faster electron transport. Thus, cycling performance of hierarchical SnO_2@SnS_2@rGO hollow spheres is prolonged, and its rate capability is greatly enhanced. Such hierarchical hollow core−shell structure can be generalized to other materials and find wide applications in high-performance energy storage devices.

■ ASSOCIATED CONTENT

Supporting Information

The Supporting Information is available free of charge on the ACS Publications website at DOI: 10.1021/acsami.5b06765.

XRD patterns and N_2 adsorption/desorption isotherms of the as-prepared SnO_2 hollow spheres, SnS_2 nanosheets, and hierarchical SnO_2@SnS_2 hollow spheres; SEM images of SnS_2 nanosheets; EDS mapping and corresponding EDS line scan of hierarchical SnO_2@SnS_2 hollow spheres and hierarchical SnO_2@SnS_2@rGO hollow spheres, respectively; CV curves and galvanostatic charge−discharge profiles of the first three cycles of the SnO_2 hollow spheres and SnS_2 nanosheets; comparison of cycling performances of hierarchical SnO_2@SnS_2@rGO hollow spheres with those of other SnO_2- or SnS_2-based nanostructured electrodes reported in the literature (PDF)

■ AUTHOR INFORMATION

Corresponding Author

*E-mail: ywang@lsu.edu. Fax: +1-225-578-9162. Tel: +1-225-578-8577.

Notes

The authors declare no competing financial interest.

■ ACKNOWLEDGMENTS

This work is supported by the Research Enhancement Award (REA) and Research Awards Program (RAP) sponsored by LaSPACE. The authors also want to acknowledge the Shared Instrumentation Facility (SIF) at LSU for XRD and SEM analyses.

■ REFERENCES

(1) Chu, S.; Majumdar, A. Opportunities and Challenges for a Sustainable Energy Future. *Nature* **2012**, *488*, 294−303.

(2) Tarascon, J. M.; Armand, M. Issues and Challenges Facing Rechargeable Lithium Batteries. *Nature* **2001**, *414*, 359−367.

(3) Li, X. L.; Gu, M.; Hu, S. Y.; Kennard, R.; Yan, P. F.; Chen, X. L.; Wang, C. M.; Sailor, M. J.; Liu, J. Mesoporous Silicon Sponge as an Anti-pulverization Structure for High-Performance Lithium-ion Battery Anodes. *Nat. Commun.* **2014**, *5*, 4105.

(4) Dunn, B.; Kamath, H.; Tarascon, J. M. Electrical Energy Storage for the Grid: a Battery of Choices. *Science* **2011**, *334*, 928−935.

(5) Yoshino, A. The Birth of the Lithium-Ion Battery. *Angew. Chem., Int. Ed.* **2012**, *51*, 5798−5800.

(6) Wang, J. J.; Luo, C.; Mao, J. F.; Zhu, Y. J.; Fan, X. L.; Gao, T.; Mignerey, A. C.; Wang, C. S. Solid-State Fabrication of SnS_2/C Nanospheres for High-Performance Sodium Ion Battery Anode. *ACS Appl. Mater. Interfaces* **2015**, *7*, 11476−11481.

(7) Zhao, K. N.; Liu, F. N.; Niu, C. J.; Xu, W. W.; Dong, Y. F.; Zhang, L.; Xie, S. M.; Yan, M. Y.; Wei, Q. L.; Zhao, D. Y.; Mai, L. Q. Graphene Oxide Wrapped Amorphous Copper Vanadium Oxide with Enhanced Capacitive Behavior for High-Rate and Long-Life Lithium-Ion Battery Anodes. *Adv. Sci.* **2015**, n/a.

(8) Liu, N.; Lu, Z. D.; Zhao, J.; McDowell, M. T.; Lee, H. W.; Zhao, W. T.; Cui, Y. A Pomegranate-Inspired Nanoscale Design for Large-Volume-Change Lithium Battery Anodes. *Nat. Nanotechnol.* **2014**, *9*, 187−192.

(9) Xie, Z. Q.; Ellis, S.; Xu, W. W.; Dye, D.; Zhao, J. Q.; Wang, Y.; Novel, A. Preparation of Core-Shell Electrode Materials via Evaporation-induced Self-Assembly of Nanoparticles for Advanced Li-ion Batteries. *Chem. Commun.* **2015**, DOI: 10.1039/C5CC05577F.

(10) Armand, M.; Tarascon, J. M. Building Better Batteries. *Nature* **2008**, *451*, 652−657.

(11) Xie, Z. Q.; Eikhuemelo, H.; Zhao, J. Q.; Cain, C.; Xu, W. W.; Wang, Y. Ni and Fe Dual-Doped $Li_4Mn_5O_{12}$ Spinels as Cathode Materials for High-Voltage Li-ion Batteries. *J. Electrochem. Soc.* **2015**, *162*, A1523−A1529.

(12) Bruce, P. G.; Freunberger, S. A.; Hardwick, L. J.; Tarascon, J. M. Li-O_2 and Li-S Batteries with High Energy Storage. *Nat. Mater.* **2012**, *11*, 19−29.

(13) Chan, C. K.; Peng, H.; Liu, G.; McIlwrath, K.; Zhang, X. F.; Huggins, R. A.; Cui, Y. High-Performance Lithium Battery Anodes Using Silicon Nanowires. *Nat. Nanotechnol.* **2008**, *3*, 31−35.

(14) Liu, S. Y.; Lu, X.; Xie, J.; Cao, G. S.; Zhu, T. J.; Zhao, X. B. Preferential c-Axis Orientation of Ultrathin SnS_2 Nanoplates on Graphene as High-Performance Anode for Li-Ion Batteries. *ACS Appl. Mater. Interfaces* **2013**, *5*, 1588−1595.

(15) Kang, B.; Ceder, G. Battery Materials for Ultrafast Charging and Discharging. *Nature* **2009**, *458*, 190−193.

(16) Xie, Z. Q.; Zhao, J. Q.; Wang, Y. One-Step Solvothermal Synthesis of Sn Nanoparticles Dispersed in Ternary Manganese-Nickel-Cobalt Carbonate as Superior Anode Materials for Lithium Ion Batteries. *Electrochim. Acta* **2015**, *174*, 1023−1029.

(17) Lee, K. T.; Jung, Y. S.; Oh, S. M. Synthesis of Tin-encapsulated Spherical Hollow Carbon for Anode Material in Lithium Secondary Batteries. *J. Am. Chem. Soc.* **2003**, *125*, 5652−5653.

(18) Besenhard, J. O.; Yang, J.; Winter, M. Will Advanced Lithium-Alloy Anodes Have a Chance in Lithium-ion Batteries? *J. Power Sources* **1997**, *68*, 87−90.

(19) Huang, J. Y.; Zhong, L.; Wang, C. M.; Sullivan, J. P.; Xu, W.; Zhang, L. Q.; Mao, S. X.; Hudak, N. S.; Liu, X. H.; Subramanian, A.; Fan, H. Y.; Qi, L.; Kushima, A.; Li, J. In Situ Observation of the Electrochemical Lithiation of a Single SnO_2 Nanowire Electrode. *Science* **2010**, *330*, 1515−1520.

(20) Chen, P.; Su, Y.; Liu, H.; Wang, Y. Interconnected Tin Disulfide Nanosheets Grown on Graphene for Li-Ion Storage and Photocatalytic Applications. *ACS Appl. Mater. Interfaces* **2013**, *5*, 12073−12082.

(21) Aravindan, V.; Jinesh, K. B.; Rajiv, R. P.; Kale, V. S.; Madhavi, S. Atomic Layer Deposited (ALD) SnO_2 Anodes with Exceptional Cycleability for Li-Ion Batteries. *Nano Energy* **2013**, *2*, 720−725.

(22) Zhang, L.; Zhao, K. N.; Xu, W. W.; Dong, Y. F.; Xia, R.; Liu, F. N.; He, L.; Wei, Q. L.; Yan, Y. M.; Mai, M. L. Integrated SnO_2 Nanorod Array with Polypyrrole Coverage for High-Rate and Long-Life Lithium Batteries. *Phys. Chem. Chem. Phys.* **2015**, *17*, 7619−7623.

(23) Liu, Z. X.; Deng, H. Q.; Mukherjee, P. P. Evaluating Pristine and Modified SnS_2 as a Lithium-Ion Battery Anode: A First-Principles Study. *ACS Appl. Mater. Interfaces* **2015**, *7*, 4000−4009.

(24) Chen, J.; Cheng, F. Y. Combination of Lightweight Elements and Nanostructured Materials for Batteries. *Acc. Chem. Res.* **2009**, *42*, 713−723.

(25) Park, M. S.; Wang, G. X.; Kang, Y. M.; Wexler, D.; Dou, S. X.; Liu, H. K. Preparation and Electrochemical Properties of SnO_2 Nanowires for Application in Lithium-Ion Batteries. *Angew. Chem.* **2007**, *119*, 764−767.

(26) Xu, W. W.; Zhao, K. N.; Niu, C. J.; Zhang, L.; Cai, Z. Y.; Han, C. H.; He, L.; Shen, T.; Yan, M. Y.; Qu, L. B.; Mai, L. Q. Heterogeneous Branched Core−Shell SnO_2−PANI Nanorod Arrays with Mechanical Integrity and Three Dimentional Electron Transport for Lithium Batteries. *Nano Energy* **2014**, *8*, 196−204.

(27) Lou, X. W.; Wang, Y.; Yuan, C. L.; Lee, J. Y.; Archer, L. A. Template-free Synthesis of SnO_2 Hollow Nanostructures with High Lithium Storage Capacity. *Adv. Mater.* **2006**, *18*, 2325−2329.

(28) Kim, H.; Cho, J. Hard Templating Synthesis of Mesoporous and Nanowire SnO_2 Lithium Battery Anode Materials. *J. Mater. Chem.* **2008**, *18*, 771−775.
(29) Wang, C.; Zhou, Y.; Ge, M. Y.; Xu, X. B.; Zhang, Z. L.; Jiang, J. Z. Large-Scale Synthesis of SnO_2 Nanosheets with High Lithium Storage Capacity. *J. Am. Chem. Soc.* **2009**, *132*, 46−47.
(30) Jeong, J. M.; Choi, B. G.; Lee, S. C.; Lee, K. G.; Chang, S. J.; Han, Y. K.; Lee, Y. B.; Lee, H. U.; Kwon, S.; Lee, G.; Lee, C. S.; Huh, Y. S. Hierarchical Hollow Spheres of Fe_2O_3@Polyaniline for Lithium Ion Battery Anodes. *Adv. Mater.* **2013**, *25*, 6250−6255.
(31) Wang, D.; Xin, H. L.; Hovden, R.; Wang, H. S.; Yu, Y. C.; Muller, D. A.; DiSalvo, F. J.; Abruña, H. D. Structurally Ordered Intermetallic Platinum−Cobalt Core−Shell Nanoparticles with Enhanced Activity and Stability as Oxygen Reduction Electrocatalysts. *Nat. Mater.* **2013**, *12*, 81−87.
(32) An, Q. Y.; Zhang, P. F.; Wei, Q. L.; He, L.; Xiong, F. Y.; Sheng, J. Z.; Wang, Q. Q.; Mai, L. Q. Top-down fabrication of three-dimensional porous V_2O_5 hierarchical microplates with tunable porosity for improved lithium battery performance. *J. Mater. Chem. A* **2014**, *2*, 3297−3302.
(33) Liang, C. D.; Dudney, N. J.; Howe, J. Y. Hierarchically Structured Sulfur/Carbon Nanocomposite Material for High-Energy Lithium Battery. *Chem. Mater.* **2009**, *21*, 4724−4730.
(34) Sun, Y. M.; Hu, X. L.; Luo, W.; Huang, Y. H. Self-Assembled Hierarchical MoO_2/Graphene Nanoarchitectures and Their Application as a High-Performance Anode Material for Lithium-Ion Batteries. *ACS Nano* **2011**, *5*, 7100−7107.
(35) Zhang, Y. C.; Zhen, N. D.; Kun, W. L.; Ming, Z.; Dionysios, D. D. High-Performance Visible-Light-Driven SnS_2/SnO_2 Nanocomposite Photocatalyst Prepared via In situ Hydrothermal Oxidation of SnS_2 Nanoparticles. *ACS Appl. Mater. Interfaces* **2011**, *3*, 1528−1537.
(36) Wang, W. W.; Zhu, Y. J.; Yang, L. X. ZnO-SnO_2 Hollow Spheres and Hierarchical Nanosheets: Hydrothermal Preparation, Formation Mechanism, and Photocatalytic Properties. *Adv. Funct. Mater.* **2007**, *17*, 59−64.
(37) Mai, L. Q.; Yang, F.; Zhao, Y. L.; Xu, X.; Xu, L.; Luo, Y. Z. Hierarchical $MnMoO_4$/$CoMoO_4$ Heterostructured Nanowires with Enhanced Supercapacitor Performance. *Nat. Commun.* **2011**, *2*, 381.
(38) Zhang, Y. D.; Zhu, P. Y.; Huang, L. L.; Xie, J.; Zhang, S. C.; Cao, G. S.; Zhao, X. B. Few-Layered SnS_2 on Few-Layered Reduced Graphene Oxide as Na-Ion Battery Anode with Ultralong Cycle Life and Superior Rate Capability. *Adv. Funct. Mater.* **2015**, *25*, 481−489.
(39) Zhou, T. F.; Pang, W. K.; Zhang, C. F.; Yang, J. P.; Chen, Z. X.; Liu, H. K.; Guo, Z. P. Enhanced sodium-ion battery performance by structural phase transition from two-dimensional hexagonal-SnS_2 to orthorhombic-SnS. *ACS Nano* **2014**, *8*, 8323−8333.
(40) Qu, B. H.; Ma, C. Z.; Ji, G.; Xu, C. H.; Xu, J.; Meng, Y. S.; Wang, T. H.; Lee, J. Y. Layered SnS_2-Reduced Graphene Oxide Composite-A High-Capacity, High-Rate, and Long-Cycle Life Sodium-Ion Battery Anode Material. *Adv. Mater.* **2014**, *26*, 3854−3859.
(41) Seo, J. W.; Jang, J. T.; Park, S. W.; Kim, C.; Park, B.; Cheon, J. W. Two-Dimensional SnS_2 Nanoplates with Extraordinary High Discharge Capacity for Lithium Ion Batteries. *Adv. Mater.* **2008**, *20*, 4269−4273.
(42) Liang, J. F.; Wei, W.; Zhong, D.; Yang, Q. L.; Li, L. D.; Guo, L. One-Step In Situ Synthesis of SnO_2/Graphene Nanocomposites and Its Application as an Anode Material for Li-ion Batteries. *ACS Appl. Mater. Interfaces* **2012**, *4*, 454−459.
(43) Jiang, X.; Yang, X. L.; Zhu, Y. H.; Shen, J. H.; Fan, K. C.; Li, C. Z. In Situ Assembly of Graphene Sheets-Supported SnS_2 Nanoplates into 3D Macroporous Aerogels for High-Performance Lithium Ion Batteries. *J. Power Sources* **2013**, *237*, 178−186.
(44) Zhang, L.; Zhang, G. Q.; Wu, H. B.; Yu, L.; Lou, X. W. Hierarchical Tubular Structures Constructed by Carbon-Coated SnO_2 Nanoplates for Highly Reversible Lithium Storage. *Adv. Mater.* **2013**, *25*, 2589−2593.
(45) Zhai, C. X.; Du, N.; Zhang, H.; Yu, J. X.; Yang, D. R. Multiwalled Carbon Nanotubes Anchored with SnS_2 Nanosheets as High-Performance Anode Materials of Lithium-ion Batteries. *ACS Appl. Mater. Interfaces* **2011**, *3*, 4067−4074.
(46) Sathish, M.; Mitani, S.; Tomai, T.; Honma, I. Ultrathin SnS_2 Nanoparticles on Graphene Nanosheets: Synthesis, Characterization, and Li-Ion Storage Applications. *J. Phys. Chem. C* **2012**, *116*, 12475−12481.
(47) Wu, Q.; Jiao, L. F.; Du, J.; Yang, J. Q.; Guo, L. J.; Liu, Y. C.; Wang, Y. J.; Yuan, H. T. One-Pot Synthesis of Three-Dimensional SnS_2 Hierarchitectures as Anode Material for Lithium-Ion Batteries. *J. Power Sources* **2013**, *239*, 89−93.

DOI: 10.1021/acsami.5b06765
ACS Appl. Mater. Interfaces 2015, 7, 22533−22541